Lattice Boltzmann simulations of nonequilibrium fluctuations in a nonideal binary mixture

Daniele Belardinelli, Mauro Sbragaglia, and Roberto Benzi
Department of Physics & INFN, University of Rome "Tor Vergata", Via della Ricerca Scientifica 1, 00133, Rome, Italy

Sergio Ciliberto
Laboratoire de Physique de Ecole Normale Superieure de Lyon (CNRS UMR5672), 46 Allée d'Italie, 69364, Lyon, France

(Received 5 August 2018; published 3 June 2019)

In recent years the lattice Boltzmann (LB) methodology has been fruitfully extended to include the effects of thermal fluctuations. So far, all studied cases pertain to equilibrium fluctuations, i.e., fluctuations with respect to an equilibrium background state. In this paper we take a step further and present results of fluctuating LB simulations of a binary mixture confined between two parallel walls in the presence of a constant concentration gradient in the wall-to-wall direction. This is a paradigmatic setup for the study of nonequilibrium (NE) fluctuations, i.e., fluctuations with respect to a nonequilibrium state. We analyze the dependence of the structure factors for the hydrodynamical fields on the wave vector $\boldsymbol{q}$ in both the directions parallel and perpendicular to the walls, highlighting the long-range ($\sim|\boldsymbol{q}|^{-4}$) nature of correlations in the NE framework. Results at the small scales (high wave numbers) quantitatively agree with the predictions of fluctuating hydrodynamics without fitting parameters. At larger scales (low wave numbers), however, results show finite-size effects induced by confinement and call for further studies aimed at controlling boundary conditions in the fluctuating LB framework as well as compressibility effects. Moreover, in the presence of a nonideal equation of state of the mixture, we also observe that the (spatially homogeneous) average pressure changes, due to a genuinely new contribution triggered by NE fluctuations. These NE pressure effects are studied at changing the system size and the concentration gradient. Taken all together, we argue that the results of this article are useful and instrumental to boost the applicability of the fluctuating LB methodology in the framework of NE fluctuations, possibly in conjunction with experiments.

DOI: 10.1103/PhysRevE.99.063302

I. INTRODUCTION

The equations of *fluctuating hydrodynamics* supplement the deterministic equations of hydrodynamics with the effect of thermal fluctuations [1]. In a nutshell, the key idea is that whenever scales of observations are small enough, thermal fluctuations cannot be ignored anymore and the nonequilibrium (NE) fluxes in the conservation equations (i.e., diffusion, viscous, etc.) need to be promoted to stochastic variables. By linearizing with respect to a homogeneous background and applying the fluctuation dissipation theorem (FDT), one obtains the structure factors for the hydrodynamical fields in agreement with the corresponding statistical mechanics predictions [2]. Away from criticality, correlations of hydrodynamical fields such as mass density and velocity come out to be short-ranged, and the experimental observations with light scattering and neutron scattering techniques confirm such predictions [3–5]. The assumption of full (thermodynamic) equilibrium of the background system greatly simplifies the theoretical approach to the study of thermal fluctuations, but is actually inappropriate in many situations where we have mechanical equilibrium even in the presence of temperature or concentration gradients. This may be the case of a Rayleigh-Bénard cell [6,7] or the case of a binary mixture under the effect of an external field [8–12]. For such systems, the theory of equilibrium thermal fluctuations can be extended [13] to predict fluctuations with respect to a nonequilibrium steady state. In general, NE effects are promoted by two sources: One source is the "mode" coupling between the fluctuating velocity and the background inhomogeneous scalar field under consideration, the temperature in single-component fluids [14–19], and both the temperature and the concentration for mixtures [20–22]. Another source can be identified in the spatial inhomogeneity of the thermal noise, due to the proportionality of the noise correlations to the temperature [23–26], as stated by FDT. Typically, the effects induced by inhomogeneity in the noise are negligible with respect to the mode coupling effect [27]. The mode coupling effect causes the small-scale behavior of scalar fluctuations to be divergent as $\sim|\boldsymbol{q}|^{-4}$, with $\boldsymbol{q}$ being the Fourier wave vector. This was first obtained in Ref. [14] in the framework of nonequilibrium statistical mechanics and later assessed in the framework of fluctuating hydrodynamics [15,19]. Experimental confirmations followed [6–9,12,28]. We emphasize that NE fluctuations cause long-range correlation effects; similar long-range correlation effects are absent in equilibrium situations, except close to criticality [29]. Moreover, the long-range nature of the NE effects causes fluctuation-induced forces. This feature has been extensively discussed in the literature [30–35]. Similar NE pressure effects have also been studied in the nonlinear Navier-Stokes equations with imposed shear rate [36–39], where the NE effects are triggered by the nonlinear coupling between the imposed shear rate and the flow itself.

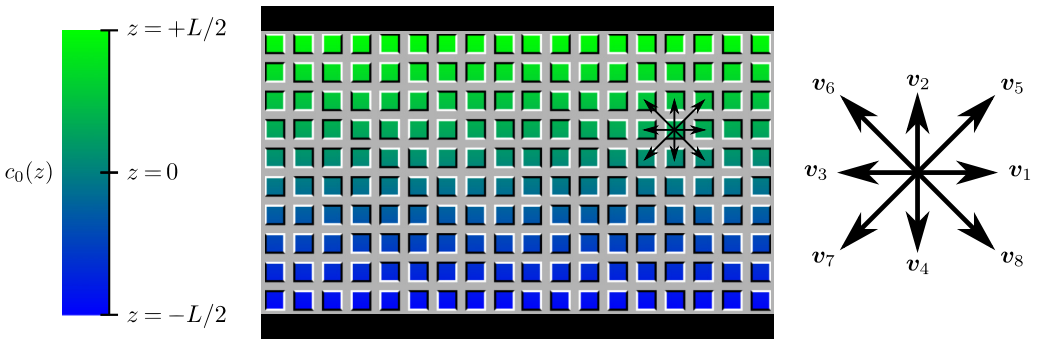

FIG. 1. Setup for the numerical simulations. The wall-to-wall distance is L and we take the convention that $z = 0$ indicates the center of the channel. A linear concentration background profile $c_0(z) = 1/2 + z\nabla c_0$ is imposed, corresponding to a constant concentration gradient ∇c_0 in the vertical direction. The vectors $\boldsymbol{v}_{1-8}$, together with $\boldsymbol{v}_0 \equiv \boldsymbol{0}$, act as lattice links in the D2Q9 LB simulations.

Thermal fluctuations become relevant at mesoscales, where many complex hydrodynamic phenomena occur, like, for example, the motion of nonideal (NI) interfaces [40], the coupling between colloidal particles and the fluid [41,42], the rheology of vesicles and red blood cells [43–45], and the acoustic-magnetic effect in magnetic fluids [46]. The need of understanding complex hydrodynamic phenomena at mesoscales naturally sets a compelling case for the development of suitably designed numerical methods. Beyond the numerical simulations based on the continuum equations of hydrodynamics [47,48], in recent years mesoscale simulations based on the *lattice Boltzmann* (LB) [49,50] have been proposed [51–53]. The LB method stands out due to its remarkable capability of handling complex boundary conditions and NI fluids with phase transitions and segregation [54–58]; hence, the LB coupled with thermal fluctuations is a promising pathway for realizing powerful mesoscale simulation methods. The idea of including noise in LB, in fact, has constituted an active research field of the recent years [51–53,59–62]. All these implementations, however, consider hydrodynamical systems fluctuating around a state in full equilibrium. The aim of the present paper is to explore the applicability of the fluctuating LB in the context of NE fluctuations. While none of the approaches proposed in the literature [51–53,59–62] can be trivially extended to the case with temperature gradients in the background, in Ref. [62] it is discussed how to formulate noise in multicomponent systems, even in presence of an inhomogeneous background concentration $c_0(\boldsymbol{r})$. Numerical simulations showed convincing agreement between the numerically evaluated equilibrium structure factors and the theoretical predictions. The latter, which can be obtained directly in the kinetic framework (see Ref. [62]), coincide with the predictions of fluctuating hydrodynamics. However, this is obviously not enough to prove convergence of fluctuating LB toward fluctuating hydrodynamics. Indeed, the stochastic noise terms break one of the basic assumptions of Chapman-Enskog theory (i.e., having fields slowly varying in space and time). Hence, the coincidence of theoretical results (kinetic framework versus hydrodynamics framework) seems like a lucky case, possibly valid in homogeneous cases. Hence, investigating NE in LB simulations is also a further way to highlight the convergence of fluctuating LB toward fluctuating hydrodynamics. The article is organized as follows. In Sec. II the system and its governing equations are presented. The used methodology is described in Sec. III. The numerical results, both in equilibrium and out of equilibrium, are discussed and compared with the theoretical predictions in Sec. IV. We conclude in Sec. V. The Appendix recalls some relevant definitions and results on the structure factors.

II. SYSTEM

In this paper we study the problem of NE fluctuations by considering a two-dimensional binary mixture confined between two walls in the presence of a constant concentration gradient ∇c_0 in the wall-to-wall direction (see Fig. 1). The reference fluctuating hydrodynamical equations for density $\delta\rho = \rho - \bar{\rho}$, concentration $\delta c = c - c_0$, and velocity $\delta\boldsymbol{U} = (U_x, U_z)$ fluctuations are

$$\partial_t \delta\rho + \bar{\rho}\boldsymbol{\nabla}\cdot\delta\boldsymbol{U} = 0, \tag{1}$$

$$\bar{\rho}(\partial_t \delta c + U_z \nabla c_0) = \bar{\rho} D \nabla^2 \delta c - \boldsymbol{\nabla}\cdot\boldsymbol{J}, \tag{2}$$

$$\bar{\rho}\partial_t \delta\boldsymbol{U} = -\boldsymbol{\nabla}\delta P + \bar{\rho}\nu(\nabla^2\delta\boldsymbol{U} + \boldsymbol{\nabla}\boldsymbol{\nabla}\cdot\delta\boldsymbol{U}) - \boldsymbol{\nabla}\cdot\boldsymbol{\Pi}, \tag{3}$$

where δP is the pressure fluctuation, while $\bar{\rho}$, D and ν are reference values for total mass density, mass diffusion coefficient and kinematic viscosity, respectively. Equations (1), (2), and (3) describe, respectively, conservation of total mass, diffusion of one species into the other, and momentum balance, in their linearized form [see Eqs. (17)–(19)]. The terms $\boldsymbol{J}$ and $\boldsymbol{\Pi}$ are the stochastic contributions to the deterministic equations of hydrodynamics in a Langevin-like approach [63–66]. Specifically, $\boldsymbol{J}$ is a stochastic flux and $\boldsymbol{\Pi}$ is a stochastic stress tensor satisfying FDT:

$$\langle J_i(\boldsymbol{r}, t) J_j(\boldsymbol{r}', t')\rangle = 2k_{\mathrm{B}} T \bar{\rho} D \chi \delta_{ij} \delta(\boldsymbol{r} - \boldsymbol{r}')\delta(t - t'), \tag{4}$$

$$\langle \Pi_{ij}(\boldsymbol{r}, t) \Pi_{kl}(\boldsymbol{r}', t')\rangle = 2k_{\mathrm{B}} T \bar{\rho} \nu \Delta_{ijkl} \delta(\boldsymbol{r} - \boldsymbol{r}')\delta(t - t'), \tag{5}$$

where δ_{ij} is the Kronecker delta, $\Delta_{ijkl} = \delta_{ik}\delta_{jl} + \delta_{il}\delta_{jk}$, k_{B} the Boltzmann constant and T the temperature, while χ indicates the inverse osmotic susceptibility: $\chi^{-1} = (\partial\mu/\partial c)_{P,T}$, with μ the chemical potential and P the fluid pressure. If Eqs. (1)–(3) are integrated in time, then the construction of the noise ensures that the proper thermal stationary state, characterized by some average properties, is reached in the limit of large times. Such a characterization will be given in Sec. IV.

We remark that, in the context of Langevin-type equations, the term "average" refers to the ensemble average over all the possible trajectories and is equivalent to the canonical ensemble average, provided that Eqs. (4) and (5) are satisfied. The very same technique is used to introduce fluctuations in the LB algorithm, as explained in the next section.

III. METHODOLOGY

The basic idea behind the LB methodology is to derive the equations of hydrodynamics from the more fundamental kinetic theory [67]. In this section we briefly review the fluctuating multicomponent LB model that we use. Extensive details are reported in Ref. [62]. The model does not consider directly the hydrodynamic fields, but considers a kinetic description of a multicomponent fluid with two species, say A and B, having mass densities ρ^{A} and ρ^{B}. The corresponding total mass density is indicated with $\rho = \rho^{\mathrm{A}} + \rho^{\mathrm{B}}$, while mass concentration is conventionally taken as $c = \rho^{\mathrm{A}}/\rho$.

A. General framework

The LB method makes use of a set of Q distribution functions $f_l^{\mathrm{S}}(\boldsymbol{r}, t)$ $(l = 0, \ldots, Q-1)$, representing the number of particles of the species $\mathrm{S} = \mathrm{A}, \mathrm{B}$ at time t in an elementary lattice cell of unit volume around the position $\boldsymbol{r}$ moving with velocity $\boldsymbol{v}_l$. Mass densities are recovered as $\rho^{\mathrm{S}} = \sum_l f_l^{\mathrm{S}}$ [68]. One then introduces the (isotropic) lattice spacing Δr and the time interval Δt to rescale positions and times, respectively. Coherently, velocities are rescaled by $\Delta r/\Delta t$. Dimensionless variables will be noted in the same way as the variables themselves. In this way, while t varies on the natural set, the velocities $\boldsymbol{v}_l$ act as links connecting the lattice points $\boldsymbol{r}$ (see Fig. 1). The LB evolution is described by the following algorithm:

$$f_l^{\mathrm{S}}(\boldsymbol{r} + \boldsymbol{v}_l, t+1) = f_l^{\mathrm{S}}(\boldsymbol{r}, t) + R_l^{\mathrm{S}}(\boldsymbol{r}, t). \tag{6}$$

Here, R_l^{S} is the responsible for the change of f_l^{S} when moving along the link $\boldsymbol{v}_l$ in a time step. It is better written in terms of the moments m_a^{S} $(a = 0, \ldots, Q-1)$, which are defined by the following invertible transformation [62]:

$$m_a^{\mathrm{S}} = \sum_l T_{al} f_l^{\mathrm{S}}, \quad f_l^{\mathrm{S}} = w_l \sum_a \frac{T_{al}}{N_a} m_a^{\mathrm{S}}. \tag{7}$$

In Table I it is reported the chosen set of T_{al} for the D2Q9 lattice used in the simulations. This is a two-dimensional lattice with $Q = 9$ velocities (see Fig. 1): $\boldsymbol{v}_0 = (0,0)$, $\boldsymbol{v}_1 = (1,0) = -\boldsymbol{v}_3$, $\boldsymbol{v}_2 = (0,1) = -\boldsymbol{v}_4$, $\boldsymbol{v}_5 = (1,1) = -\boldsymbol{v}_7$, $\boldsymbol{v}_6 = (-1,1) = -\boldsymbol{v}_8$, the associated weights being $w_0 = 4/9$, $w_{1-4} = 1/9$, and $w_{5-8} = 1/36$. The normalization constants are obtained as $N_a = \sum_l w_l T_{al}^2$. In particular, lattice mass and momentum densities are given by

$$\rho^{\mathrm{S}} = m_0^{\mathrm{S}} = \sum_l f_l^{\mathrm{S}}$$

and

$$\boldsymbol{j}^{\mathrm{S}} = \left(j_x^{\mathrm{S}}, j_z^{\mathrm{S}}\right) = \left(m_1^{\mathrm{S}}, m_2^{\mathrm{S}}\right) = \sum_l \boldsymbol{v}_l f_l^{\mathrm{S}},$$

TABLE I. Moments set for the D2Q9 model used in the LB simulations. The index S of the species has been omitted. As the set of velocities is finite, the set of T_{al} forms a basis. The moments m_a are computed according to Eq. (7). They relax toward their respective asymptotic values according to a time scale $1/\lambda_a$. The first three rows cover the conserved moments.

a	T_{al}	m_a	$m_a^{\mathrm{eq}}(\rho, \boldsymbol{U})$	λ_a
0	1	ρ	ρ	λ_0
1	$(\boldsymbol{v}_l)_x$	j_x	ρU_x	λ_{d}
2	$(\boldsymbol{v}_l)_z$	j_z	ρU_z	λ_{d}
3	$3\lvert\boldsymbol{v}_l\rvert^2 - 2$	e	$3\rho\lvert\boldsymbol{U}\rvert^2$	λ_e
4	$(\boldsymbol{v}_l)_x^2 - (\boldsymbol{v}_l)_z^2$	Σ_{ww}	$\rho(U_x^2 - U_z^2)$	λ_{s}
5	$(\boldsymbol{v}_l)_x(\boldsymbol{v}_l)_z$	Σ_{xz}	$\rho U_x U_z$	λ_{s}
6	$(3\lvert\boldsymbol{v}_l\rvert^2 - 4)(\boldsymbol{v}_l)_x$	Q_x	0	λ_Q
7	$(3\lvert\boldsymbol{v}_l\rvert^2 - 4)(\boldsymbol{v}_l)_z$	Q_z	0	λ_Q
8	$9\lvert\boldsymbol{v}_l\rvert^4 - 15\lvert\boldsymbol{v}_l\rvert^2 + 2$	ϵ	0	λ_ϵ

respectively. While the lattice mass densities coincide with their physical counterpart, the physical baricentric velocity $\boldsymbol{U}$ is constructed as [62]

$$\rho\boldsymbol{U} = (\rho U_x, \rho U_z) = \boldsymbol{j}^{\mathrm{A}} + \boldsymbol{j}^{\mathrm{B}} + \tfrac{1}{2}\rho\boldsymbol{a}. \tag{8}$$

The additional term is a correction related to the time discretization and involves the effective body-force density $\rho\boldsymbol{a}$ acting on the fluid. We can write $\rho\boldsymbol{a} = \rho^{\mathrm{A}}\boldsymbol{a}^{\mathrm{A}} + \rho^{\mathrm{B}}\boldsymbol{a}^{\mathrm{B}}$ and decompose each term in the sum of nonideal (NI) and nonequilibrium (NE) contributions by writing for each species $\boldsymbol{a}^{\mathrm{S}} = \boldsymbol{a}_{\mathrm{NI}}^{\mathrm{S}} + \boldsymbol{a}_{\mathrm{NE}}^{\mathrm{S}}$. The former is constructed on the lattice and takes the form [69–73]

$$\boldsymbol{a}_{\mathrm{NI}}^{\mathrm{A}}(\boldsymbol{r}, t) = -G\sum_l w_l \boldsymbol{v}_l \rho^{\mathrm{B}}(\boldsymbol{r} + \boldsymbol{v}_l, t), \tag{9}$$

and an analogous expression holds for $\boldsymbol{a}_{\mathrm{NI}}^{\mathrm{B}}$, having B replaced by A on the right-hand side. The positive constant G is the same for both the species and is a tunable parameter in the model [74]. It regulates the intensity of interactions between the two fluids, which are assumed to be separately ideal (in the expression of $\boldsymbol{a}_{\mathrm{NI}}^{\mathrm{A}}$ only ρ^{B} appears). This produces a NI contribution in the equation of state [see Eq. (16) below]. The NE contribution is chosen in such a way that it imposes a concentration gradient $\nabla c_0 = (0, \nabla c_0)$ in the steady state, which is important for the study of NE effects:

$$\boldsymbol{a}_{\mathrm{NE}}^{\mathrm{A}} = \tfrac{1}{3}(0, \nabla c_0/c), \tag{10}$$

where the prefactor has been conveniently chosen equal to the lattice speed of sound for the D2Q9 model, that is 1/3 [67]. The analogous expression for $\boldsymbol{a}_{\mathrm{NE}}^{\mathrm{B}}$ is obtained by replacing $\nabla c_0/c$ with $-\nabla c_0/(1-c) = \nabla c_0/(c-1)$. Notice that the momentum balance and consequently the pressure are unaffected by the NE forcing, since

$$\rho^{\mathrm{A}}\boldsymbol{a}_{\mathrm{NE}}^{\mathrm{A}} + \rho^{\mathrm{B}}\boldsymbol{a}_{\mathrm{NE}}^{\mathrm{B}} = \boldsymbol{0}. \tag{11}$$

In this way, the NE acceleration Eq. (10) gives a contribution in the diffusion current proportional to $\rho\nabla c_0$ [see Eq. (18) below], thus fixing $\nabla c = \nabla c_0$ in the stationary steady state [75]. Moments for $a = 3, \ldots, 5$ are related to the viscous stress tensor, while higher order moments have no hydrodynamical

counterpart and constitute the so-called "ghost" sector (see Table I). Close to a *local* equilibrium state only the first moments contribute, as we can write $m_a^{\rm S} = m_a^{\rm eq}(\rho^{\rm S}, \boldsymbol{U})$, with the equilibrium hydrodynamical moments $m_a^{\rm eq}(\rho, \boldsymbol{U})$ given in Table I. With these ingredients, the last term in Eq. (6) can be written as

$$R_l^{\rm S} = w_l \sum_a \frac{T_{al}}{N_a}\left(C_a^{\rm S} + F_a^{\rm S} + \xi_a^{\rm S}\right). \tag{12}$$

The first term in the round brackets models the relaxation toward the *local* equilibrium:

$$C_a^{\rm S} = \lambda_a^{\rm S}\left[m_a^{\rm eq}(\rho^{\rm S}, \boldsymbol{U}) - m_a^{\rm S}\right]. \tag{13}$$

The dimensionless constants $\lambda_a^{\rm S}$ are the lattice relaxation frequencies, $1/\lambda_a^{\rm S}$ being the corresponding lattice relaxation times. This is the multiple relaxation times (MRT) generalization of the celebrated BGK (for Bhatnagar, Gross, and Krook [76]) form of the Boltzmann collision integral. All the $\lambda_a^{\rm S}$ are tunable parameters of the model, with some restrictions imposed by the request of mass and momentum conservations. Since $m_0^{\rm eq}(\rho^{\rm S}, \boldsymbol{U}) = m_0^{\rm S} = \rho^{\rm S}$, mass conservation is ensured for each species separately, independently on the actual value of $\lambda_0^{\rm S}$. Instead, the second argument of the equilibrium distribution in Eq. (13) is the baricentric velocity $\boldsymbol{U}$ of Eq. (8), allowing in this way the diffusion of one species into the other. Conservation of *total* momentum is then enforced by conveniently choosing

$$\lambda_{1,2}^{\rm S} = \lambda_{\rm d},$$

where the lattice diffusion relaxation frequency $\lambda_{\rm d}$ is the same for both the species. Similarly, the lattice relaxation frequencies associated to the shear moments Σ_{ww} and Σ_{xz} ($a = 4, 5$, see Table I) are chosen as

$$\lambda_{4,5}^{\rm S} = \lambda_{\rm s},$$

with the lattice shear relaxation frequency $\lambda_{\rm s}$ being the same for both the species.

The second term in the round brackets of Eq. (12) models the action of the interactions between the fluid particles. The first order moments ($a = 1, 2$) are given by

$$\left(F_1^{\rm S}, F_2^{\rm S}\right) = \rho^{\rm S}\boldsymbol{a}^{\rm S}.$$

We omit the expression of the moments of order higher than one, for shortness, by remarking that they must be included for a proper simulation of a nonhomogeneous fluctuating system [62].

The last term in the round brackets of Eq. (12) accounts for thermal fluctuations. These are modelled with zero-mean Gaussian random variables, uncorrelated in time and with constant covariances (which can however depend on $\boldsymbol{r}$). The derivation of the precise expression of the noise covariances has been achieved in Ref. [62]. It makes use of the FDT directly applied at the kinetic level. The covariance matrix appears to be diagonal in both moments [77] and space, as well as in time by construction, allowing us to write

$$\left\langle \xi_a^{\rm S}(\boldsymbol{r}, t)\xi_{a'}^{\rm S'}(\boldsymbol{r}', t')\right\rangle = \langle \xi^{\rm S}\xi^{\rm S'}\rangle_a \delta_{a,a'}\delta_{\boldsymbol{r},\boldsymbol{r}'}\delta_{t,t'}.$$

The quantities $\xi_a^{\rm S}$ are arranged in the same way as the moments $m_a^{\rm S}$. In particular, the stochastic injections of mass and momentum densities are $\rho_\xi^{\rm S} = \xi_0^{\rm S}$ and $\boldsymbol{j}_\xi^{\rm S} = (\xi_1^{\rm S}, \xi_2^{\rm S})$, respectively. As a direct consequence of mass conservation for each species it results that

$$\langle \xi^{\rm S}\xi^{\rm S'}\rangle_0 = 0,$$

coherently with an identically vanishing $\rho_\xi^{\rm S}$. Momentum, instead, is not conserved separately for each species, due to diffusion effects. However, total momentum in conserved, so that $\boldsymbol{j}_\xi^{\rm A} + \boldsymbol{j}_\xi^{\rm B}$ must be identically vanishing. Coherently, it is found that

$$\langle \xi^{\rm S}\xi^{\rm S}\rangle_{1,2} = -\langle \xi^{\rm A}\xi^{\rm B}\rangle_{1,2} = (2 - \lambda_{\rm d})\lambda_{\rm d} k_{\rm B} T \frac{\rho^{\rm A}\rho^{\rm B}}{\rho}. \tag{14}$$

Higher-order noise correlations have also to be taken into account. The only nonvanishing are for ${\rm S} = {\rm S}'$:

$$\langle \xi^{\rm S}\xi^{\rm S}\rangle_a = 3\left(2 - \lambda_a^{\rm S}\right)\lambda_a^{\rm S} N_a k_{\rm B} T \rho^{\rm S} \text{ for } a = 3, \ldots, 8. \tag{15}$$

The factors $\langle \xi^{\rm S}\xi^{\rm S'}\rangle_a$ would depend on space through their dependence on the background fields $\rho^{\rm S}$. However, to focus on the mode coupling effects [27], we mainly performed simulations by keeping the $\rho^{\rm S}$ in Eqs. (14) and (15) equal to their reference values. The effect of inhomogeneities in the $\langle \xi^{\rm S}\xi^{\rm S'}\rangle_a$ will also be highlighted in this study. Of central role in the derivation of the previous noise covariances are the properties of the *noiseless* ($\xi_a^{\rm S} \equiv 0$) stationary state reached by the system. This is assumed to have the *local* equilibrium form $m_a^{\rm S} = m_a^{\rm eq}(\rho^{\rm S}, \boldsymbol{0}) = \rho^{\rm S}\delta_{a,0}$, so that $C_a^{\rm S} = 0$. Thus, by summing Eq. (6) over the species, using Eqs. (11) and (9), and performing the continuum limit (formally, $\boldsymbol{v}_l \to \boldsymbol{0}$), we get $\boldsymbol{\nabla}\rho = -G\boldsymbol{\nabla}(\rho^{\rm A}\rho^{\rm B})$. This can be written in the form $\boldsymbol{\nabla}P = \boldsymbol{0}$, allowing us to deduce the equation of state $P = P(\rho, c)$ for the system at hand:

$$\begin{aligned} P &= \tfrac{1}{3}(\rho^{\rm A} + \rho^{\rm B}) + \tfrac{1}{3}G\rho^{\rm A}\rho^{\rm B} \\ &= \tfrac{1}{3}\rho + \tfrac{1}{3}G\rho^2 c(1 - c). \end{aligned} \tag{16}$$

The ideal equation of state $P = \rho/3$ is recovered by setting $G = 0$; recall that the factor $1/3$ equals the D2Q9 lattice speed of sound [67]. By applying the Chapman-Enskog procedure and treating the stochastic terms as generic external forces, one can prove [78] that the fluctuating hydrodynamic equations of a binary mixture with total mass density ρ, baricentric velocity $\boldsymbol{U}$ and mass concentration c are recovered [79] (the superscript $^{\intercal}$ denotes transposition):

$$\partial_t\rho + \boldsymbol{\nabla}\cdot(\rho\boldsymbol{U}) = 0, \tag{17}$$

$$\rho(\partial_t c + \boldsymbol{U}\cdot\boldsymbol{\nabla}c) = \boldsymbol{\nabla}\cdot[\rho D\boldsymbol{\nabla}(c - c_0) - \boldsymbol{J}], \tag{18}$$

$$\rho(\partial_t\boldsymbol{U} + \boldsymbol{U}\cdot\boldsymbol{\nabla}\boldsymbol{U}) = -\boldsymbol{\nabla}P + \boldsymbol{\nabla}\cdot[\rho\nu(\boldsymbol{\nabla}\boldsymbol{U} + \boldsymbol{\nabla}\boldsymbol{U}^{\intercal}) - \boldsymbol{\Pi}], \tag{19}$$

where $\boldsymbol{J}$ and $\boldsymbol{\Pi}$ are the noise fields whose variances are fixed by the Chapman-Enskog procedure, and thus satisfying FDT at kinetic level. The mass diffusion coefficient

$$D = \frac{1}{3}\left(\frac{1}{\lambda_{\rm d}} - \frac{1}{2}\right) \tag{20}$$

and the kinematic viscosity

$$\nu = \frac{1}{3}\left(\frac{1}{\lambda_{\rm s}} - \frac{1}{2}\right), \tag{21}$$

respectively, regulate the intensity of the diffusion fluxes and the viscous stresses [78] and are tunable in the model, by specifying λ_d and λ_s independently. Notice that the total mass density here is a dynamical variable. However, compressibility effects result to be small for the average profile, within an error of 1–2%, hence by linearizing the equations around the background state one ends up with Eqs. (1)–(3), with a reference total mass density $\bar{\rho}$ suitably chosen (see the end of next subsection).

Summarizing, we use the LB solver described in Ref. [62] to simulate the hydrodynamical equations of a binary mixture in presence of a background stationary concentration gradient. If we trust the hydrodynamical limit of the LB model, then we can assess the properties of fluctuations by changing the background gradient ∇c_0, the geometry used, the transport coefficients D and ν, and the interaction strength G that regulates the NI character of the mixture. We again remark that the fluctuating terms violate one of the basic assumptions of Chapman-Enskog theory (i.e., having fields slowly varying in space and time). We can only formally obtain Eqs. (17)–(19). Rather, the convergence toward the fluctuating hydrodynamical equations must be assessed via numerical simulations and a careful comparisons with the predictions of fluctuating hydrodynamics [32,80,81].

B. Setup

We consider a two-dimensional system with dimensions $L_x \times L$, with periodic boundary conditions in the stream-flow (x) direction and two solid walls located at $z = \pm L/2$. The two-dimensional choice is done to make the many computations affordable at changing L up to few tens of grid points. Indeed, the solutions of fluctuating hydrodynamics assume infinitely long parallel walls [13]; hence, for a given L, the stream-flow lengthscale L_x needs to be large enough to prevent spurious effects induced by periodicity. Regarding the boundary conditions, we choose the midway bounce back rule for the LB kinetic populations [82]: apart from small discrete effects, these provide a no-slip boundary condition for the tangential velocity ($U_x = 0$) in absence of fluctuations. We also enforced exactly a zero normal velocity at the wall ($U_z = 0$) at every time-step by properly readjusting the rest population at the wall. Regarding the boundary conditions on the concentration field, we impose that the densities of both components at the wall are equal to the neighboring fluid nodes [83]. Both the no-slip boundary condition and the conditions on the species densities (hence the boundary condition on concentration) are obviously changed by thermal fluctuations. To the best of the authors' knowledge there is no systematic study on the effects induced by thermal fluctuations on the LB boundary conditions and their hydrodynamic manifestations. A systematic study is surely warranted for the future. However, for the purposes of the present paper, we remark that boundary conditions affect the NE spectra only at large scales [32,80,81], while the small-scale behavior is rather independent of the boundary conditions used. Moreover, regarding the large-scales, there are various solutions of fluctuating hydrodynamics that report the effects of hydrodynamic boundary conditions [32,80,81]. Thus, if from one side we can assess the universality in the small-scale behavior, as a bonus we can also explore the importance of the boundary conditions by direct comparisons against analytical solutions available.

From now on, when writing $\bar{\rho}$ we will mean that reference value for the total mass density such that, for given values of L_x and L, the product $\bar{\rho} L_x L$ gives the total mass, which is exactly conserved by the algorithm. All the simulations are performed in such a way that

$$\bar{c}_0 \equiv c_0(z = 0) = \tfrac{1}{2},$$

and we take $\bar{c}_0$ as the reference value for the concentration.

IV. RESULTS AND DISCUSSIONS

All the numerical results discussed in the following sections will be reported in LB units. In particular, in those units we set $\bar{\rho} = 1$. We then set the other relevant physical parameters, such as concentration gradient, wall-to-wall separation, thermal energy, and kinematic viscosity, to some "reference" base values in all the simulations, unless when explicitly varied. In both Secs. IV A and IV B the reference values are $\nabla c_0 = 0.01$, $L = 32$, $k_B T = 10^{-4}$, $\nu = 0.16667$, $D = 0.00427$ as well as $G = 0$ (ideal binary mixture). The choice $L_x = 4L$ is enough to obtain negligible spurious effects for wavenumbers as small as $1/L$. In Sec. IV C, to better highlight the NE effects induced to the average pressure, which increase with both the wall-to-wall distance and temperature (see Fig. 10 below), we change L and $k_B T$ into $L = 64$ and $k_B T = 5 \times 10^{-4}$. We also switch on nonideal interactions, when needed, by setting $G = 0.3$; this guarantees that phase separation never occurs.

A. Equilibrium fluctuations ($\nabla c_0 = 0$)

The model that we use has already been extensively validated in unconfined homogeneous situations in Ref. [62]. Equilibrium fluctuations can be studied in Fourier space through the structure factors of the velocity and concentration fluctuations, respectively, $S_{U_{x,z}}(\boldsymbol{q})$ and $S_c(\boldsymbol{q})$ (see the Appendix), where

$$\boldsymbol{q} = (q_x, q_z)$$

is the wave vector. It is well known [13] that for equilibrium fluctuations in unbounded domains the structure factors of both velocity and concentration fluctuations are independent of the wave vector. More quantitatively,

$$S_{U_{x,z}}(\boldsymbol{q}) = \langle |U_{x,z}(\boldsymbol{q})|^2 \rangle = \frac{k_B T}{\bar{\rho}}, \tag{22}$$

$$S_c(\boldsymbol{q}) = \langle |\delta c(\boldsymbol{q})|^2 \rangle = 3 \frac{k_B T}{\bar{\rho}} \bar{c}_0 (1 - \bar{c}_0). \tag{23}$$

This corresponds to delta-like correlations in real space:

$$\langle U_{x,z}(z) U_{x,z}(0) \rangle = \frac{k_B T}{\bar{\rho}} \delta_{z,0}, \tag{24}$$

$$\langle \delta c(z) \delta c(0) \rangle = 3 \frac{k_B T}{\bar{\rho}} \bar{c}_0 (1 - \bar{c}_0) \delta_{z,0}. \tag{25}$$

However, we will use confined simulations with wall boundary conditions for the NE fluctuations ($\nabla c_0 \neq 0$), it is therefore important to conduct a preliminary characterization of

the equilibrium fluctuations ($\nabla c_0 = 0$) in such confined situations. We thus considered a *homogeneous* system ($\nabla c_0 = 0$) confined in a channel with fixed wall-to-wall separation L, and performed simulations at changing k_BT in the range 10^{-6}–10^{-4}. The measured structure factors in both the streamflow, $\boldsymbol{q} = (q, 0)$, and the wall-to-wall, $\boldsymbol{q} = (0, q)$, directions are shown in Fig. 2 on varying dimensionless wave numbers,

$$\tilde{q} = qL, \tag{26}$$

whose smallest acceptable value for the wall-to-wall direction is 2π, by construction, while such a limitation is absent for the streamflow direction. The measured structure factors are close to the reference theory values in unconfined situations given in Eqs. (22) and (23). Notice that the velocity structure factors reported in Fig. 2 do not exhibit the anisotropy typical of a divergenceless field. In particular, for a divergenceless velocity the scalar product $\boldsymbol{q} \cdot \delta\boldsymbol{U}(\boldsymbol{q}) = q_x U_x(q_x, q_z) + q_z U_z(q_x, q_z)$ identically vanishes, and consequently $U_x(q, 0) = U_z(0, q) = 0$ identically. This is not the case here, since the fluid at hand is not exactly incompressible. Some underestimates and anisotropy are observed, that we attribute to the presence of walls, which are not contemplated in Eqs. (22) and (23). Results reported in Fig. 2 will serve as a reference case to quantify the importance of non equilibrium fluctuations. As shown in the following section, these properties are maintained by the velocities even in presence of a non zero concentration gradient, while the concentration itself exhibits long-range spatial correlations (see Fig. 4).

B. Nonequilibrium fluctuations ($\nabla c_0 \neq 0$)

In this section we start by describing the NE fluctuations. In Fig. 3 we report results for the structure factors for the velocity and concentration fluctuations. We observe that the structure factors for the velocities $U_{x,z}$ (top and central panels) do not show any substantial change with respect to the corresponding equilibrium situation reported in Fig. 2. For the fluctuations in the concentration field δc (bottom panel), instead, the structure factors are strongly anisotropic and mode-dependent, which markedly contrasts the observations in the equilibrium situation. Correspondingly, the effect on the correlations in real space is highlighted in Fig. 4: the two-point correlation function for the velocity (data shown only for the stream-flow velocity U_x) does not show any net NE contribution; in contrast, the NE contribution of the two-point correlation for the concentration highlights a correlation length that essentially spans the whole system size. To characterize such NE fluctuations on a more quantitative basis, we therefore continue our analysis for the concentration field c in a "parallel flow approximation," i.e., by taking the Fourier mode along the stream-flow direction, $\boldsymbol{q} = (q, 0)$. To facilitate a comparison with the existing literature on NE fluctuations we adopt the commonly used decomposition [13]

$$S_c(q, 0) = 3\frac{k_BT}{\bar{\rho}}\bar{c}_0(1 - \bar{c}_0)[1 + \phi\tilde{S}_{\text{NE}}(qL)], \tag{27}$$

where

$$\phi = \frac{1}{3}\frac{L^4}{\bar{c}_0(1 - \bar{c}_0)}\frac{(\nabla c_0)^2}{(\nu + D)D}. \tag{28}$$

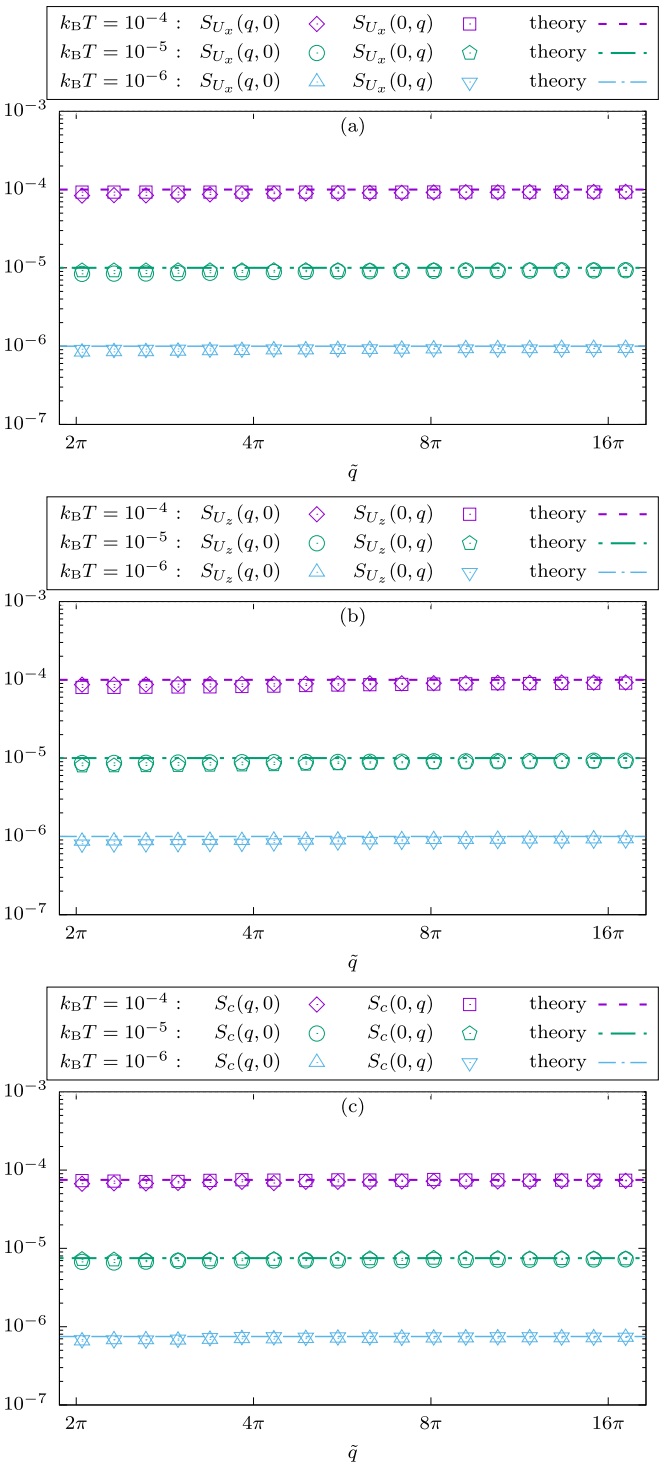

FIG. 2. Spectra of fluctuations of hydrodynamical fields around an equilibrium background ($\nabla c_0 = 0$). Top panel: Velocity in the streamflow (x) direction; theoretical prediction in Eq. (22). Central panel: Velocity in the wall-to-wall (z) direction; theoretical prediction in Eq. (22). Bottom panel: Concentration fluctuations; theoretical prediction in Eq. (23). All the theoretical predictions refer to unbounded fluids. In all cases, the viscosity and diffusivity have been fixed to their reference values (cf. Sec. IV).

Starting from the data reported in Fig. 3 and the decomposition Eq. (27), we extracted the function $\phi\tilde{S}_{\text{NE}}(\tilde{q})$. The results

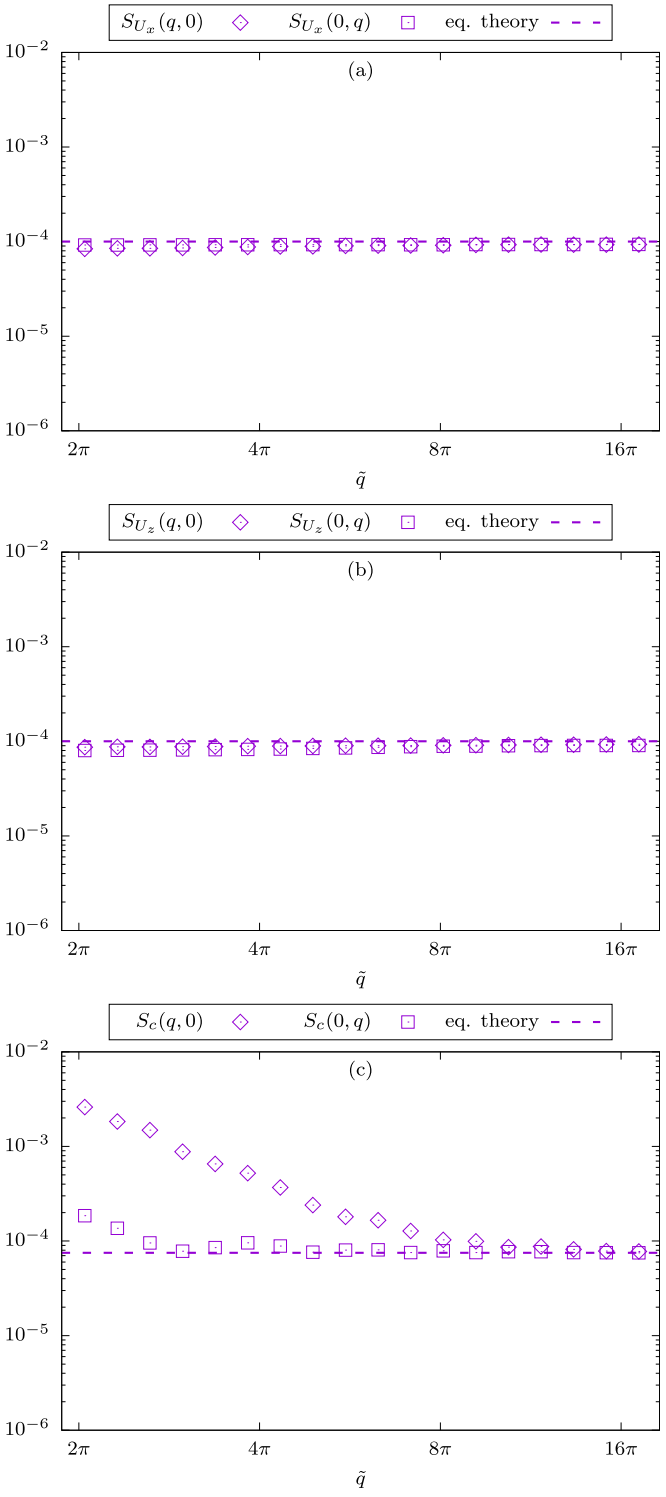

FIG. 3. Spectra of fluctuations of hydrodynamical fields around a NE background ($\nabla c_0 \neq 0$). Top panel: Velocity in the streamflow (x) direction; equilibrium theoretical prediction in Eq. (22). Central panel: Velocity in the wall-to-wall (z) direction; equilibrium theoretical prediction in Eq. (22). Bottom panel: Concentration fluctuations; equilibrium theoretical prediction in Eq. (23). In all cases, the simulation parameters have been fixed to their reference values (cf. Sec. IV).

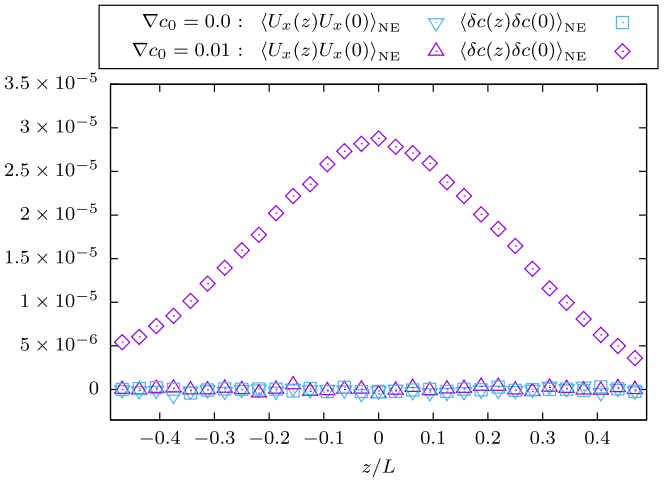

FIG. 4. Real space NE correlations of velocity and concentration fluctuations. They are obtained by subtracting to the measured correlations the equilibrium values reported in Eqs. (24) and (25). The simulation parameters have been fixed to their reference values (cf. Sec. IV).

are reported in Fig. 5. At small scales ($\tilde{q} \gg 1$) we observe the power-law scaling $\tilde{S}_{\rm NE}(\tilde{q}) \sim \tilde{q}^{-4}$. This is perfectly in agreement with the expected power-law behavior $\tilde{S}_{\rm NE}(\tilde{q}) = \tilde{q}^{-4}$ predicted by the theory of NE fluctuations, which can be obtained from the equations of hydrodynamics linearized around a constant concentration gradient profile, i.e., Eqs. (1)–(3). We emphasize that we just used the decomposition Eq. (27) and added *no additional* fitting parameters. We checked the goodness of the asymptotic behavior by separately changing the concentration gradient ∇c_0, the wall-to-wall separation L and the kinematic viscosity ν, while keeping the diffusion coefficient D unvaried. This can be done in the simulations thanks to the MRT generalization of the BGK model [see Eq. (13)], which allows to set different relaxation frequencies for different moments [see Eqs. (20) and (21)]. The plots reported in Fig. 5 show changes in agreement with the corresponding change of ϕ in Eq. (28). We also checked that the product $\phi\tilde{S}_{\rm NE}(\tilde{q})$ does not depend on $k_{\rm B}T$ in the range 10^{-6}–10^{-4}, thus confirming the linear dependence of $S_c(q,0)$ on temperature in the factorization Eq. (27). These results provide a very strong indication that the fluctuating LB methodology is quantitatively able to reproduce the small scale behavior of NE correlations obtained from fluctuating hydrodynamics in presence of NE fluctuations [30–35].

At the small scales where the prediction of fluctuating hydrodynamics well matches the results of the simulations (cf. Fig. 5), we inspected the effect of the spatial dependence of the noise correlations in Eqs. (14) and (15). Some authors before investigated the relative importance of mode-coupling effects and nonhomogeneity in noise [27,84]. In particular, they show that for a case with temperature (with thermal diffusivity D_T in place of diffusivity D) the importance of the mode coupling effect with respect to the inhomogeneity in noise scales inversely proportional to the quantity $(\nu + D_T)D_T$. In other words, if the inhomogeneous noise is switched-on in the simulations, the diffussivity and the viscosity need to be properly chosen to guarantee that results of fluctuating hydrodynamics with homogeneous noise hold. To highlight this, we conducted various numerical simulations at changing

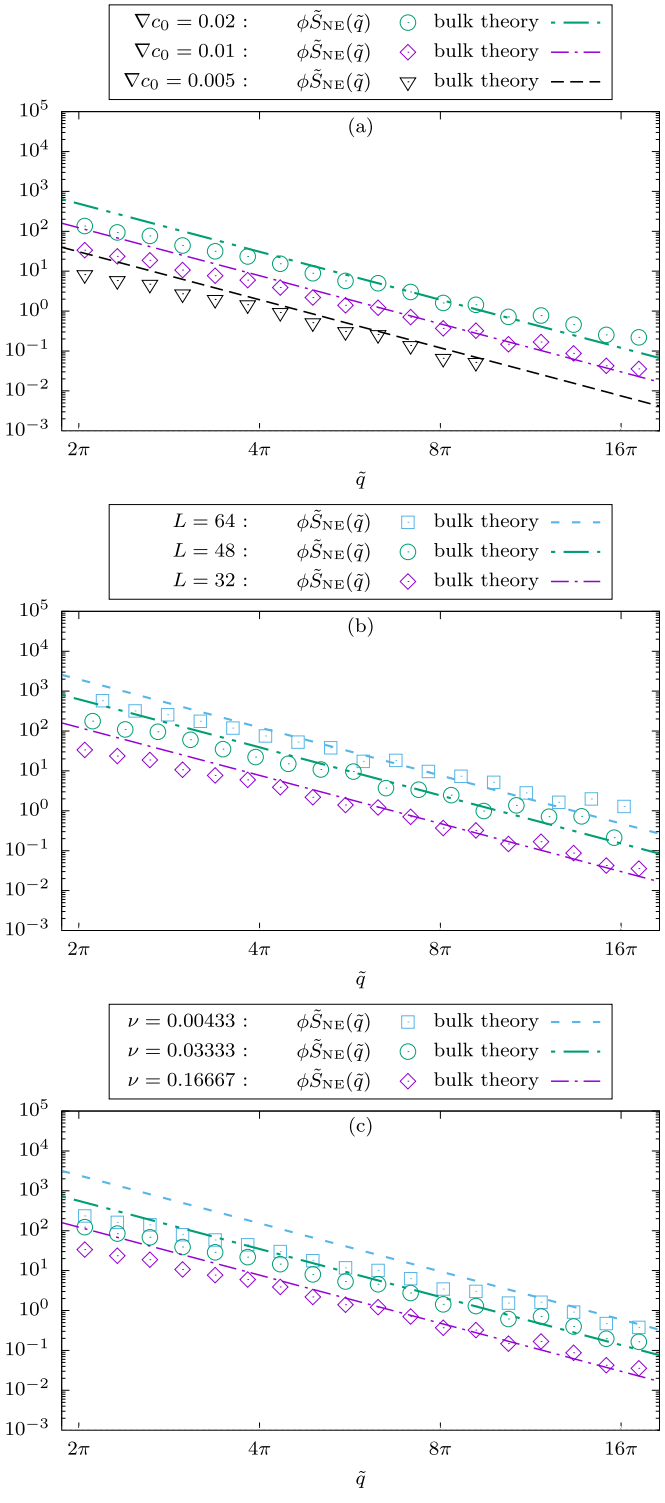

FIG. 5. Nonequilibrium structure factor contribution [see Eqs. (27) and (28)] as a function of the dimensionless wave number $\tilde{q}$ [see Eq. (26)]; the theoretical prediction, corresponding to $\tilde{S}_{\rm NE}(\tilde{q}) = \tilde{q}^{-4}$, is obtained from Eqs. (1)–(3) for unbounded systems. Top panel: NE structure factor contribution for different concentration gradients ∇c_0. Central panel: NE structure factor contribution for different wall-to-wall separations L. Bottom panel: NE structure factor contribution for different kinematic viscosities ν. The simulation parameters not given in the legends are detailed in Sec. IV.

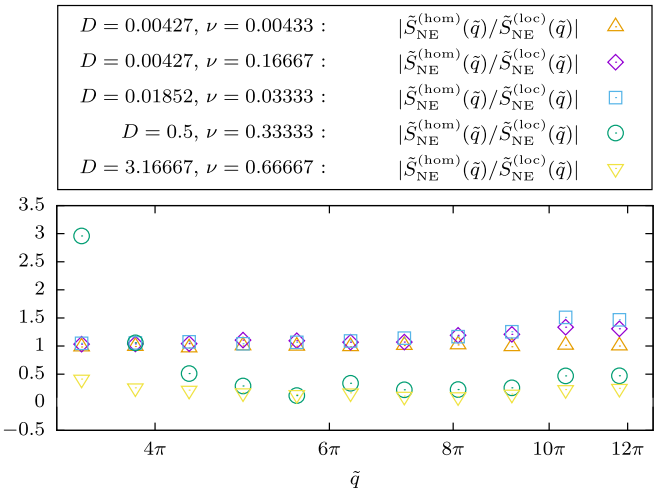

FIG. 6. We report the ratio between the nonequilibrium structure factors computed by implementing the noise according to Eqs. (14) and (15) and using the constant reference value for the mass densities (hom) and local space-dependent (loc) density. Different transport coefficient are considered. The simulation parameters not given in the legends are detailed in Sec. IV.

both ν and D, from small values to larger values. In Fig. 6 we reported the ratio between $\phi\tilde{S}_{\rm NE}^{\rm (hom)}(\tilde{q})$ and $\phi\tilde{S}_{\rm NE}^{\rm (loc)}(\tilde{q})$, i.e., the nonequilibrium structure factors computed by implementing the noise according to Eqs. (14) and (15) and using constant reference values for the mass densities (hom) and those obtained using the local (loc) values. We see that when both the transport coefficients (ν and D) are very small, the two simulations provide the same results. Instead, by increasing both transport coefficients different results are observed. This is just a qualitative statement, as a quantitative study requires further numerical, as well as theoretical analysis. We remark, however, that the effects induced by inhomogeneity in the noise are typically negligible with respect to the mode coupling effect for many practical purposes (details are given in Ref. [27]).

Going at smaller $\tilde{q}$ we observe in Fig. 5 that the power-law scaling $\sim\tilde{q}^{-4}$ becomes progressively underestimated by the numerically computed $\tilde{S}_{\rm NE}(\tilde{q})$. This is attributed to finite-size effects induced by confinement. Indeed, due to the long-range nature of NE spatial correlations, NE structure factors are necessarily affected by the boundary conditions. There are various papers aimed at the quantitative characterization of $\tilde{S}_{\rm NE}(\tilde{q})$ in presence of boundary conditions [32,80,81]. The results of these calculations share the common feature that the power-law behavior $\sim\tilde{q}^{-4}$ is approached only at very small scales, i.e., $\tilde{S}_{\rm NE}(\tilde{q}) \sim \tilde{q}^{-4}$ only for $\tilde{q} \to \infty$. The small-$\tilde{q}$ behavior strongly depends on the boundary conditions used for both velocity and concentration. In what follows, we discuss three analytical (or semi-analytical) expressions for $\tilde{S}_{\rm NE}(\tilde{q})$ that can be gathered from the literature. All of them treat the wall as impenetrable:

$$U_z|_{z=\pm L/2} = 0.$$

This condition is strictly imposed in all the simulations performed. One can then impose either no-slip (NS) or free-slip

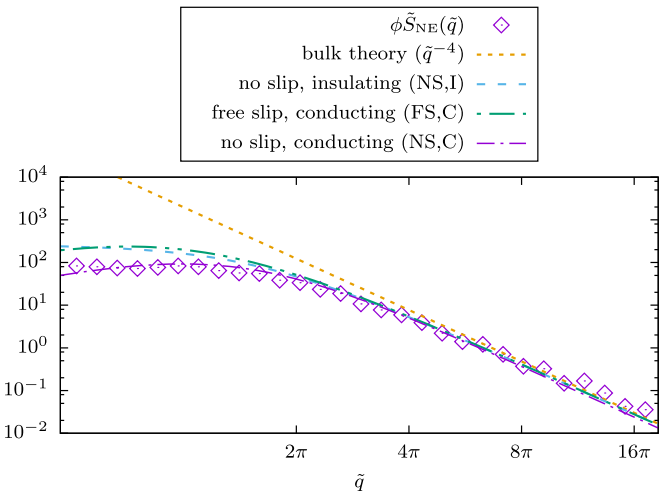

FIG. 7. Nonequilibrium structure factor contribution as a function of the dimensionless wavenumber $\tilde{q}$ [see Eq. (26)]. Different analytical formulas are checked, dependently on the boundary conditions Eq. (29). The choice of the simulation parameters is detailed in Sec. IV.

(FS) boundary conditions for U_x, and independently either insulating (I) or conducting (C) boundary conditions for δc:

$$\begin{aligned} &\text{(NS,I)}: (U_x, \partial_z \delta c)|_{z=\pm L/2} = \mathbf{0}, \\ &\text{(FS,C)}: (\partial_z U_x, \delta c)|_{z=\pm L/2} = \mathbf{0}, \\ &\text{(NS,C)}: (U_x, \delta c)|_{z=\pm L/2} = \mathbf{0}. \end{aligned} \tag{29}$$

Depending on the boundary conditions in Eq. (29), different expressions for $\tilde{S}_{\rm NE}(\tilde{q})$ can be found in literature, as reported explicitly in the Appendix. The solution that better fits the data reported in Fig. 7 is (NS,C). This is reasonable: we use a bounce-back for the kinetic population, thus reproducing the no-slip condition in the hydrodynamical limit; moreover, since fluctuations in the concentration are triggered by $k_{\rm B}T \ll 1$, one may also say that the conducting boundary condition fits well in those conditions where the concentration fluctuations are much smaller than the average concentration. However, we hasten to remark that a quantification of the boundary conditions with LB in presence of noise is currently missing in the literature. This surely stimulates further work in the future.

Before closing this section, some remarks on the issue of compressibility are needed. All the reported analytical results [32,80,81] are derived in the incompressible regime. The fluid velocity in our system is not divergenceless (see the discussion on the velocity structure factors reported in Fig. 2). Thus, one could wonder if compressibility plays a role. To this aim, recall that in the incompressible case the equation for U_x can be decoupled by taking the double curl of Eq. (3) and using $\boldsymbol{\nabla} \cdot \delta \boldsymbol{U} = 0$. The resulting equations for U_z and c are the starting point for the computations performed in Refs. [32,80,81]. By following the same procedure, in our case we would get additional contributions in the momentum balance involving $\boldsymbol{\nabla}(\boldsymbol{\nabla} \cdot \delta \boldsymbol{U})$, whose z-component in Fourier space reads $-q_z \boldsymbol{q} \cdot \delta \boldsymbol{U}(\boldsymbol{q})$. These contributions are identically vanishing for $\boldsymbol{q} = (q, 0)$, thus giving the same bulk equations as in the incompressible case. Notice, however, that the incompressibility condition is routinely used in formulating a "closed" boundary condition in terms of the velocity component U_z [32,80,81] and to the best of our knowledge, there is no analytical result for confined flows involving compressibility effects in the imposition of the boundary conditions. Therefore, at this stage, it is not clear how much of the observed behavior at large scales depends on compressibility effects. This point surely stimulates further research for the future.

Summarizing, the LB solver described in Ref. [62] generates a fluctuating hydrodynamical system that under the presence of a constant concentration gradient and homogeneous noise develops the typical long-range correlations characterizing NE fluctuations. Remarkably, neither fitting parameters nor corrective factors are needed to match numerics and analytical results at the small scales. Confinement effects also seem captured, although a more systematic study of the boundary conditions emerging in the simulations is needed.

C. Nonequilibrium pressures

Recent papers of the literature [30–35] supported the fact that the long-range effects deriving from NE fluctuations (see Fig. 4) cause a NE "Casimir" pressure. The rationale behind this effect hinges on the connection between the pressure and concentration fluctuations. In a nutshell, the *local* equilibrium assumption relates mass density and concentration to pressure through an equation of state $P = P(\rho, c)$ satisfying $\boldsymbol{\nabla} P = \mathbf{0}$ [see Eq. (16) for the case at hand], which is expected to be still valid in average. Fluctuations of ρ and c are then accompanied by fluctuations of P that one expects to be vanishing at linear order [19,33,35]. By keeping the first non vanishing terms, one gets [33,35]

$$P_{\rm NE}(z) = \tfrac{1}{2} A_c \langle |\delta c(z)|^2 \rangle_{\rm NE}, \tag{30}$$

where the vanishing of the linear order is used to express $\delta\rho$ in terms of δc. The constant A_c plays the role of a second order coefficient, and is a function of the background fields computed at their respective reference values. Two important comments are in order. *First*, based on the prediction for the NE pressure in Eq. (30), one would expect NE Casimir pressures to be triggered by the nonideality of the mixture [see Eq. (16)]: an ideal equation of state ($G = 0$) would just deliver $A_c = 0$ and hence $P_{\rm NE} = 0$. *Second,* the NE correlation $\langle |\delta c(z)|^2 \rangle_{\rm NE}$ may be nonhomogeneous in space, depending on the choice of the boundary conditions [32,33,35]. Thus, the resulting NE pressure in Eq. (30) is space-dependent and one may wonder how this could be reconciled with an average mechanical balance. Indeed, the mode coupling effect triggers NE effects only in the concentration fluctuations, while velocity fluctuations are unchanged (see Fig. 3); thus, one would expect the equilibrium condition of a constant (average) pressure to be recovered. As already pointed out [35], the mechanism of compensation is a NE renormalization of the background profile which provides a zero derivative of the *total* pressure. In other words, the pressure may be seen as the sum of an equilibrium contribution and the NE contribution of Eq. (30); z-dependency in the latter causes the former to be z-dependent in such a way that the total pressure has zero derivative.

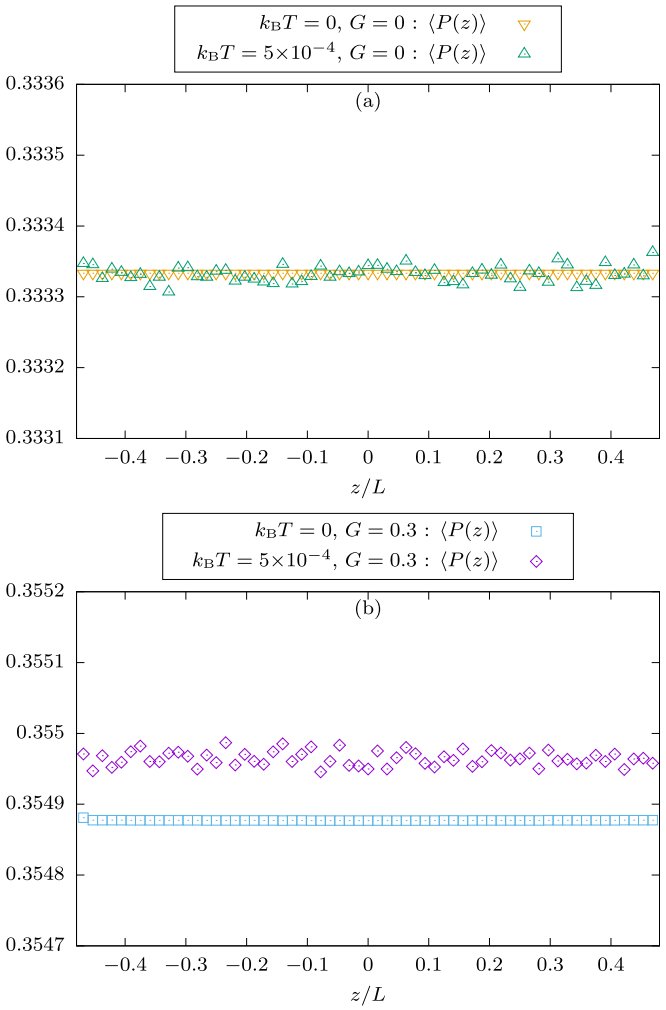

FIG. 8. Average *total* pressure. Top panel: Average total pressure for an ideal binary mixture ($G = 0$). Bottom panel: Average total pressure for a nonideal binary mixture ($G > 0$). The choice of the simulation parameters is detailed in Sec. IV.

Based on the numerical model that we used, we are in a condition to test directly these properties. The set-up to measure the NE "Casimir" pressure is the same used for the measure of the NE structure factors with the same boundary conditions. In practice, the *total* pressure is evaluated by its mechanical definition, that is as half of the trace of the pressure tensor [73], whose bulk behavior is expected to coincide with Eq. (16) in the hydrodynamical limit. Results are reported in Figs. 8 and 9 and fully confirm the above views. Specifically, we fixed a nonzero concentration gradient $\nabla c_0 = 0.01$, and we performed simulations with $k_BT > 0$ and $k_BT = 0$ for an ideal mixture ($G = 0$, Fig. 8, top panel) and for a nonideal mixture ($G > 0$, Fig. 8, bottom panel). We observed that the *total* pressure profiles are homogeneous in z and that the pressure receives a correction by thermal fluctuations *only when* $G > 0$. Only when the pressure receives a correction, the average density profile slightly changes with thermal fluctuations. This can be seen in Fig. 9, where we reported the deviation $\Delta\rho(z)$ of the average density profile with respect to its values in the noiseless case. Note that the effect on the density is quite small, and to point it out in the simulations we

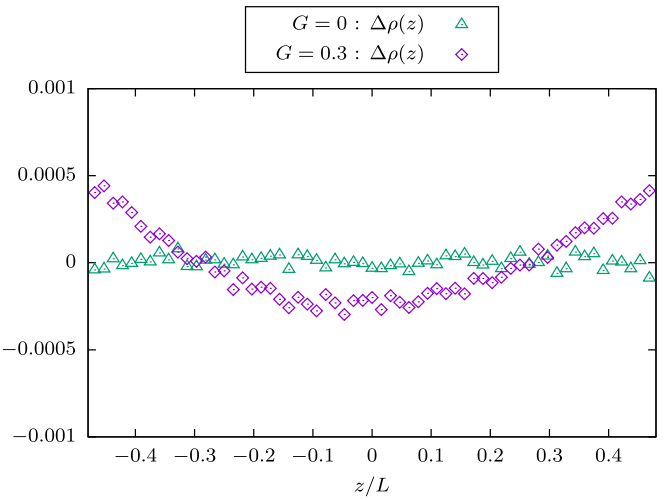

FIG. 9. Deviation of the average total mass density from it noiseless value in both the ideal ($G = 0$) and nonideal ($G > 0$) cases. The choice of the simulation parameters is detailed in Sec. IV.

had to use large L and k_BT to maximize it (see later discussion on the scaling laws of NE pressure).

These facts said, we wanted to further characterize the NE Casimir pressure from our simulations, hence we sticked with a nonideal mixture with fixed $G > 0$. The *spatial* average pressure will then depend on k_BT, L, and ∇c_0, i.e., $\overline{P} = \overline{P}(k_BT, L, \nabla c_0)$. To make progress we wanted to study the scaling properties of the NE Casimir pressure as a function of the system size L, concentration gradient ∇c_0 and k_BT. We emphasize that fluctuations are expected to induce pressure effects also in equilibrium conditions ($\nabla c_0 = 0$), and that the latter effects are particularly large close to the critical point (critical "Casimir" pressure) and decay to zero at large L [29]. For the parameters chosen [72] the critical point corresponds to $G = 2$, while we kept $G = 0.3$ in all the nonideal simulations. In such conditions thermal fluctuations only trigger some small effects in equilibrium conditions, that we detect only at the smallest L considered; however, aiming at characterizing the NE pressure at changing L, we needed to remove such small contributions. We proceeded as follows. For a given system size L, we first performed a numerical simulation in equilibrium conditions ($\nabla c_0 = 0$) without thermal fluctuation ($k_BT = 0$); we then repeated the simulation with the desired k_BT. In both simulations we have computed the average pressure and we estimated the pressure difference induced by thermal fluctuations as [85]

$$\Delta P^{\text{eq}}(k_BT, L) = \overline{P}(k_BT, L, 0) - \overline{P}(0, L, 0).$$

Then, for the desired $\nabla c_0 > 0$, we performed two other simulations without thermal fluctuations ($k_BT = 0$) and with the desired k_BT. The NE contribution to the spatial average pressure has been identified as

$$\overline{P}_{\text{NE}}(k_BT, L, \nabla c_0) = \overline{P}(k_BT, L, \nabla c_0) - \overline{P}(0, L, \nabla c_0) - \Delta P^{\text{eq}}(k_BT, L). \tag{31}$$

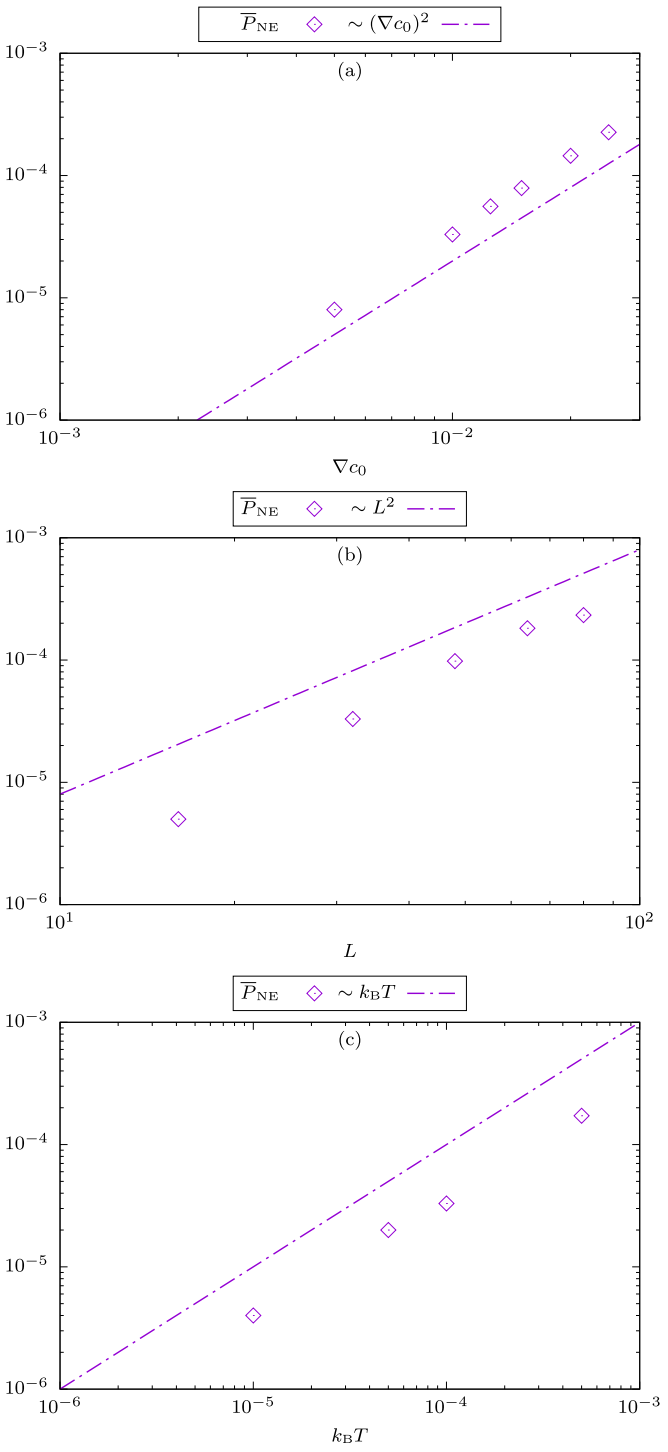

FIG. 10. Scaling laws for the NE contribution to the *spatial* average pressure computed according to Eq. (31). Top panel: NE pressure contribution as a function of the concentration gradient ∇c_0. Central panel: NE pressure contribution as a function of the wall-to-wall separation L. Bottom panel: NE pressure contribution as a function of the thermal energy $k_{\rm B}T$. The choice of the simulation parameters not given in the legends is detailed in Sec. IV.

In Fig. 10 we plot the measured $\overline{P}_{\rm NE}$ as a function of ∇c_0, L, and $k_{\rm B}T$. While the scalings $\overline{P}_{\rm NE} \sim (\nabla c_0)^2$ and $\overline{P}_{\rm NE} \sim k_{\rm B}T$ are in agreement with the theoretical predictions [30–35], the behavior of $\overline{P}_{\rm NE} \sim L^2$ reflects the two-dimensional character of the system. This can be understood by looking at the unbounded behavior $\sim|\boldsymbol{q}|^{-4}$ of $\langle|\delta c(\boldsymbol{q})|^2\rangle_{\rm NE}$ in Fourier space. Indeed, the computation of the NE average pressure from Eq. (30) requires the integration of $|\boldsymbol{q}|^{-3}$ in a two-dimensional system, in contrast with the integration of $|\boldsymbol{q}|^{-2}$ for a three-dimensional system, as those considered in Refs. [30–35]. Consequently, if an infrared cutoff proportional to L^{-1} is introduced, then a two-dimensional system furnishes $\sim L^2$, while a three-dimensional system gives $\sim L$. Predicting the offsets requires the complete control of the boundary conditions.

V. CONCLUSIONS

We applied the fluctuating lattice Boltzmann (LB) methodology described in Ref. [62] to a system out of thermodynamic equilibrium. Specifically, we considered a binary mixture confined between two parallel walls in presence of a constant concentration gradient in the wall-to-wall direction. We studied structure factors and spatial correlations of the velocity and concentration fluctuations, and found good agreement with the theoretical predictions of fluctuating hydrodynamics [13]. We further inspected the behavior of the resulting NE pressure as a function of both the concentration gradient and the wall-to-wall distance, and verified the correctness of the corresponding expected scaling laws [32,33,35], in agreement with a constant average total pressure. The results here reported naturally warrant other future quantitative studies, both numerical and theoretical. In the context of the LB methodology, the analysis of the structure factors revealed the necessity of a better control in implementing the boundary conditions in presence of thermal fluctuations. Furthermore, the extension of the Chapman-Enskog procedure to the fluctuating case is missing. In this sense, the results of this paper support the convergence of fluctuating LB toward fluctuating hydrodynamics. In the context of finite size effects in the NE fluctuations, it would be interesting to further inspect the importance of compressibility effects for analytical solutions in presence of confinement, with the aim of comparing with the LB simulations.

On a more general perspective, we remark that NE effects are continuously invoked in a variety of situations of experimental interest involving complex hydrodynamics. These include studies with colloidal suspensions [86–89], transient and enhanced diffusion effects [90–93], driven active matter [94], complex polymeric fluids [95], finite Reynolds numbers fluids [96]. In particular, for the future, it could be insightful to design experiments involving colloidal particles exhibiting a mechanical-chemical coupling with the fluid [97], in such a way that NE fluctuations effects can be indirectly reconstructed and studied from the particles trajectories. The LB methodology has proven capable of remarkable versatility in the simulation of colloidal particles [54–58], hence results of the present paper are instrumental for the use of LB as a validated methodology to support and complement experimental studies in the aforementioned direction.

APPENDIX: STRUCTURE FACTORS

In this Appendix we report the essential technical details for the computations of the structure factors of a generic scalar field $\varphi = U_x, U_z, c$. Given the wave vector $\boldsymbol{q} = (q_x, q_z)$, we started from the partial Fourier transform around a z-dependent background $\varphi_0(z)$:

$$\delta\varphi(q_x, z, t) = \frac{1}{\sqrt{L_x}} \int_0^{L_x} dx[\varphi(x, z, t) - \varphi_0(z)]e^{-iq_x x}.$$

Based on Eq. (6.30) in Ref. [13], we defined the quantity $\mathcal{C}_\varphi(q_x, z, z')$ through the equal-time mixed correlation:

$$\langle \delta\varphi(q_x, z, t)^* \delta\varphi(q_x', z', t)\rangle = \mathcal{C}_\varphi(q_x, z, z')2\pi\delta(q_x - q_x'),$$

where $\langle \dots \rangle$ indicates the ensemble average computed via the equal time average in the statistically stationary state. We then Fourier-transformed in z and z' to define the structure factor (see Eq. (31) in Ref. [80]):

$$S_\varphi(\boldsymbol{q}) = \frac{1}{L} \int_{-L/2}^{+L/2} dz dz' e^{-iq_z(z-z')} \mathcal{C}_\varphi(q_x, z, z').$$

We can also write

$$\langle \delta\varphi(\boldsymbol{q}, t)^* \delta\varphi(\boldsymbol{q}', t)\rangle = S_\varphi(\boldsymbol{q})(2\pi)^2\delta(\boldsymbol{q} - \boldsymbol{q}'),$$

which gives $S_\varphi(\boldsymbol{q}) = \langle|\delta\varphi(\boldsymbol{q}, t)|^2\rangle$ on a two-dimensional lattice, where $(2\pi)^2\delta(\boldsymbol{q} - \boldsymbol{q}')$ is replaced by $\delta_{\boldsymbol{q},\boldsymbol{q}'}$.

The decomposition Eq. (27) for the structure factor of the concentration field $\varphi = c$, computed in the stream-flow direction, $\boldsymbol{q} = (q, 0)$, can then be used to extract the NE contribution $\tilde{S}_{\rm NE}(\tilde{q})$, where $\tilde{q} = qL$. Depending on the boundary conditions at $z = \pm L/2$ [see Eq. (29)], different expressions for $\tilde{S}_{\rm NE}(\tilde{q})$ are obtained. The (NS,I) solution found in Eq. (30) of Ref. [32] is valid for $\nu \gg D$. It predicts

$$\tilde{S}_{\rm NE}^{\rm (NS,I)}(\tilde{q}) = \frac{1}{\tilde{q}^4}\left(1 + \frac{4}{\tilde{q}}\frac{1 - \cosh\tilde{q}}{\tilde{q} + \sinh\tilde{q}}\right), \qquad \nu \gg D. \tag{A1}$$

For the (FS,C) boundary conditions one can get an exact solution (see Eq. (35) in Ref. [80]):

$$\tilde{S}_{\rm NE}^{\rm (FS,C)}(\tilde{q}) = \frac{1}{\tilde{q}^4}[1 + H(\tilde{q}, 0)], \tag{A2}$$

where

$$H(\tilde{q}, 0) = \frac{1 - \cosh\tilde{q}}{4\tilde{q}\sinh\tilde{q}}\left(15 - \frac{7\tilde{q}}{\sinh\tilde{q}} + \tilde{q}^2\frac{1 - \cosh\tilde{q}}{\sinh^2\tilde{q}}\right). \tag{A3}$$

Details for (NS,C) are found in Eqs. (1), (20) and (26) of Ref. [81] (see also (7.36) in Ref. [13]). In particular, this solution comes from a Galerkin truncation of exact equations. Hence it is a semi-analytical estimate [98]. Quantitatively, it reads

$$\tilde{S}_{\rm NE}^{\rm (NS,C)}(\tilde{q}) = \frac{30}{36}\frac{\mathrm{Sc} + 1}{\mathrm{Sc} + \tilde{A}(\tilde{q})}\frac{27\tilde{q}^2}{28(\tilde{q}^2 + 10)[(\tilde{q}^2 + 12)^2 + 360]}, \tag{A4}$$

where

$$\tilde{A}(\tilde{q}) = \frac{(\tilde{q}^2 + 12)(\tilde{q}^2 + 10)}{\tilde{q}^4 + 24\tilde{q}^2 + 504}. \tag{A5}$$

[1] L. D. Landau and E. M. Lifshitz, *Course of Theoretical Physics, Vol. 6, Fluid Mechanics* (Elsevier, Amsterdam, 2013).
[2] L. E. Reichl, *A Modern Course in Statistical Physics* (John Wiley & Sons, New York, 2016).
[3] B. Berne and R. Pecora, *Dynamic Light Scattering with Applications to Biology, Chemistry, and Physics* (Wiley, New York, 1976).
[4] J. Earnshaw and R. McGivern, J. Phys. D **20**, 82 (1987).
[5] J. Earnshaw and A. McLaughlin, Proc. R. Soc. Lond. A **440**, 519 (1993).
[6] B. M. Law, P. N. Segré, R. W. Gammon, and J. V. Sengers, Phys. Rev. A **41**, 816 (1990).
[7] P. N. Segrè, R. W. Gammon, J. V. Sengers, and B. M. Law, Phys. Rev. A **45**, 714 (1992).
[8] A. Vailati and M. Giglio, Nature **390**, 262 (1997).
[9] F. Croccolo, D. Brogioli, A. Vailati, M. Giglio, and D. S. Cannell, Phys. Rev. E **76**, 041112 (2007).
[10] F. Croccolo, J. O. de Zárate, and J. Sengers, Eur. Phys. J. E **39**, 125 (2016).
[11] F. Croccolo and H. Bataller, Eur. Phys. J. E **39**, 132 (2016).
[12] A. Oprisan and A. L. Payne, Opt. Commun. **290**, 100 (2013).
[13] J. M. Ortiz de Zárate and J. V. Sengers, *Hydrodynamic Fluctuations in Fluids and Fluid Mixtures* (Elsevier, Amsterdam, 2006).
[14] T. R. Kirkpatrick, E. G. D. Cohen, and J. R. Dorfman, Phys. Rev. A **26**, 995 (1982).
[15] D. Ronis and I. Procaccia, Phys. Rev. A **26**, 1812 (1982).
[16] T. Kirkpatrick and E. Cohen, J. Stat. Phys. **33**, 639 (1983).
[17] R. Schmitz and E. Cohen, J. Stat. Phys. **39**, 285 (1985).
[18] R. Schmitz and E. Cohen, J. Stat. Phys. **40**, 431 (1985).
[19] B. Law and J. Sengers, J. Stat. Phys. **57**, 531 (1989).
[20] B. M. Law and J. C. Nieuwoudt, Phys. Rev. A **40**, 3880 (1989).
[21] J. C. Nieuwoudt and B. M. Law, Phys. Rev. A **42**, 2003 (1990).
[22] P. Segrè and J. Sengers, Physica A: Stat. Mech. Appl. **198**, 46 (1993).
[23] I. Procaccia, D. Ronis, and I. Oppenheim, Phys. Rev. Lett. **42**, 287 (1979).
[24] D. Ronis, I. Procaccia, and J. Machta, Phys. Rev. A **22**, 714 (1980).
[25] A.-M. S. Tremblay, M. Arai, and E. D. Siggia, Phys. Rev. A **23**, 1451 (1981).
[26] A.-M. Tremblay, in *Recent Developments in Nonequilibrium Thermodynamics*, edited by J. Casas-Vázquez, D. Jou, and G. Lebon (Springer, Berlin, 1984), pp. 267–315.
[27] J. M. Ortiz de Zárate and J. V. Sengers, J. Stat. Phys. **115**, 1341 (2004).
[28] D. Bedeaux, S. Kjelstrup, and J. V. Sengers, *Experimental Thermodynamics Volume X: Nonequilibrium Thermodynamics with Applications* (Royal Society of Chemistry, London, 2015), Vol. 10.
[29] A. Gambassi, J. Phys.: Conf. Ser. **161**, 012037 (2009).
[30] T. R. Kirkpatrick, J. M. Ortiz de Zárate, and J. V. Sengers, Phys. Rev. Lett. **110**, 235902 (2013).

[31] T. R. Kirkpatrick, J. M. Ortiz de Zárate, and J. V. Sengers, Phys. Rev. E **89**, 022145 (2014).

[32] J. M. Ortiz de Zárate, T. Kirkpatrick, and J. Sengers, Eur. Phys. J. E **38**, 99 (2015).

[33] T. R. Kirkpatrick, J. M. Ortiz de Zárate, and J. V. Sengers, Phys. Rev. Lett. **115**, 035901 (2015).

[34] T. R. Kirkpatrick, J. M. Ortiz de Zárate, and J. V. Sengers, Phys. Rev. E **93**, 012148 (2016).

[35] T. R. Kirkpatrick, J. M. Ortiz de Zárate, and J. V. Sengers, Phys. Rev. E **93**, 032117 (2016).

[36] J. Lutsko and J. W. Dufty, Phys. Rev. A **32**, 3040 (1985).

[37] H. Wada and S.-i. Sasa, Phys. Rev. E **67**, 065302(R) (2003).

[38] J. M. Ortiz de Zárate and J. V. Sengers, Phys. Rev. E **77**, 026306 (2008).

[39] A. Varghese, G. Gompper, and R. G. Winkler, Phys. Rev. E **96**, 062617 (2017).

[40] D. G. Aarts, M. Schmidt, and H. N. Lekkerkerker, Science **304**, 847 (2004).

[41] P. Lipowsky, M. J. Bowick, J. H. Meinke, D. R. Nelson, and A. R. Bausch, Nat. Mater. **4**, 407 (2005).

[42] T. Einert, P. Lipowsky, J. Schilling, M. J. Bowick, and A. R. Bausch, Langmuir **21**, 12076 (2005).

[43] H. Noguchi and G. Gompper, Proc. Natl. Acad. Sci. USA **102**, 14159 (2005).

[44] Y. Park, C. A. Best, T. Auth, N. S. Gov, S. A. Safran, G. Popescu, S. Suresh, and M. S. Feld, Proc. Natl. Acad. Sci. USA **107**, 1289 (2010).

[45] D. A. Fedosov, B. Caswell, and G. E. Karniadakis, Biophys. J. **98**, 2215 (2010).

[46] A. Storozhenko, A. Tantsyura, P. Ryapolov, G. Karpova, V. Polunin, and M. M. Tan, Magnetohydrodynamics **47**, 345 (2011).

[47] G. De Fabritiis, M. Serrano, R. Delgado-Buscalioni, and P. V. Coveney, Phys. Rev. E **75**, 026307 (2007).

[48] F. Balboa, J. B. Bell, R. Delgado-Buscalioni, A. Donev, T. G. Fai, B. E. Griffith, and C. S. Peskin, Multiscale Model. Simul. **10**, 1369 (2012).

[49] R. Benzi, S. Succi, and M. Vergassola, Phys. Rep. **222**, 145 (1992).

[50] S. Chen and G. D. Doolen, Annu. Rev. Fluid Mech. **30**, 329 (1998).

[51] M. Gross, M. Cates, F. Varnik, and R. Adhikari, J. Stat. Mech.: Theory Exp. (2011) P03030.

[52] B. Dünweg, U. D. Schiller, and A. J. C. Ladd, Phys. Rev. E **76**, 036704 (2007).

[53] G. Kaehler and A. J. Wagner, Phys. Rev. E **87**, 063310 (2013).

[54] B. Dünweg and A. J. Ladd, in *Advanced Computer Simulation Approaches for Soft Matter Sciences III*, edited by C. Holm and K. Kremer (Springer, Berlin, 2009), pp. 89–166.

[55] C. K. Aidun and J. R. Clausen, Annu. Rev. Fluid Mech. **42**, 439 (2010).

[56] J. Zhang, Microfluid. Nanofluid. **10**, 1 (2011).

[57] L. Chen, Q. Kang, Y. Mu, Y.-L. He, and W.-Q. Tao, Int. J. Heat Mass Transf. **76**, 210 (2014).

[58] U. D. Schiller, T. Krüger, and O. Henrich, Soft Matter **14**, 9 (2018).

[59] A. J. Ladd, J. Fluid Mech. **271**, 285 (1994).

[60] R. Adhikari, K. Stratford, M. Cates, and A. Wagner, Europhys. Lett. **71**, 473 (2005).

[61] M. Gross, R. Adhikari, M. E. Cates, and F. Varnik, Phys. Rev. E **82**, 056714 (2010).

[62] D. Belardinelli, M. Sbragaglia, L. Biferale, M. Gross, and F. Varnik, Phys. Rev. E **91**, 023313 (2015).

[63] P. Langevin, Compt. Rendus **146**, 530 (1908) [Am. J. Phys. **65**, 1079 (1997)].

[64] R. Kubo, Rep. Progr. Phys. **29**, 255 (1966).

[65] R. F. Fox, Phys. Rep. **48**, 179 (1978).

[66] R. Zwanzig, *Nonequilibrium Statistical Mechanics* (Oxford University Press, Oxford, 2001).

[67] X. Shan, X.-F. Yuan, and H. Chen, J. Fluid Mech. **550**, 413 (2006).

[68] For simplicity, we will neglect differences in molecular masses between the two species by setting each of them equal to unit.

[69] X. Shan and H. Chen, Phys. Rev. E **47**, 1815 (1993).

[70] X. Shan and H. Chen, Phys. Rev. E **49**, 2941 (1994).

[71] S. Bastea, R. Esposito, J. L. Lebowitz, and R. Marra, Phys. Rev. Lett. **89**, 235701 (2002).

[72] R. Benzi, M. Sbragaglia, S. Succi, M. Bernaschi, and S. Chibbaro, J. Chem. Phys. **131**, 104903 (2009).

[73] M. Sbragaglia and D. Belardinelli, Phys. Rev. E **88**, 013306 (2013).

[74] M. Sbragaglia, R. Benzi, L. Biferale, S. Succi, K. Sugiyama, and F. Toschi, Phys. Rev. E **75**, 026702 (2007).

[75] To allow Eq. (18) to be recovered for any value of ∇c_0 a further contribution to the acceleration must be added in the form $\boldsymbol{a}_*^{\mathrm{A}} = (1-c)(\boldsymbol{a}_{\mathrm{NI}}^{\mathrm{B}} - \boldsymbol{a}_{\mathrm{NI}}^{\mathrm{A}})$, which satisfies the relation Eq. (11), thus giving the same equation of state Eq. (16).

[76] P. L. Bhatnagar, E. P. Gross, and M. Krook, Phys. Rev. **94**, 511 (1954).

[77] For the sake of precision, we mention that off-diagonal noise correlations emerge upon discretization of the velocity space [62], which are, however, negligible for practical purposes.

[78] M. Sega, M. Sbragaglia, S. S. Kantorovich, and A. O. Ivanov, Soft Matter **9**, 10092 (2013).

[79] In the viscous stress tensor, the additional contribution $(\eta_{\mathrm{b}} - \rho\nu)\nabla\cdot\boldsymbol{U}$, containing the bulk viscosity η_{b}, vanishes thanks to the assumption $\eta_{\mathrm{b}} = \rho\nu$. This is realized with the LB when the relaxation frequencies of shear (λ_s) and bulk (λ_e) modes are the same (see Table I).

[80] J. M. Ortiz de Zárate, R. P. Cordón, and J. Sengers, Physica A: Stat. Mech. Appl. **291**, 113 (2001).

[81] J. M. Ortiz de Zárate and J. V. Sengers, Phys. Rev. E **66**, 036305 (2002).

[82] S. Succi, *The Lattice-Boltzmann Equation* (Oxford University Press, Oxford, 2001).

[83] M. Sbragaglia, K. Sugiyama, and L. Biferale, J. Fluid Mech. **614**, 471 (2008).

[84] R. Velasco and L. G. Colin, J. Phys. A: Math. Gen. **24**, 1007 (1991).

[85] In principle, pressure would be proportional to temperature through the speed of sound squared $c_s^2 \propto k_{\mathrm{B}} T$. However, c_s^2 is fixed by the choice of the lattice to be 1/3 [see Eq. (16)], resulting in a nonvanishing pressure at zero temperature. More precisely, $k_{\mathrm{B}} T$ parametrizes here the intensity of thermal fluctuations [see Eqs. (14) and (15)] at the actual scale of observation, the latter being chosen in such a way that the speed of sound squared is of order one.

[86] F. Croccolo, D. Brogioli, A. Vailati, M. Giglio, and D. S. Cannell, Ann. N.Y. Acad. Sci. **1077**, 365 (2006).
[87] A. Oprisan, S. Oprisan, and A. Teklu, Appl. Opt. **49**, 86 (2010).
[88] F. Giavazzi, G. Savorana, A. Vailati, and R. Cerbino, Soft Matter **12**, 6588 (2016).
[89] A. Oprisan, A. Rice, S. A. Oprisan, C. Giraudet, and F. Croccolo, Eur. Phys. J. E **40**, 14 (2017).
[90] A. Donev, J. B. Bell, A. de la Fuente, and A. L. Garcia, Phys. Rev. Lett. **106**, 204501 (2011).
[91] A. Donev, T. G. Fai, and E. Vanden-Eijnden, J. Stat. Mech.: Theor. Exp. (2014) P04004.
[92] R. Cerbino, Y. Sun, A. Donev, and A. Vailati, Sci. Rep. **5**, 14486 (2015).
[93] P. Baaske, H. Bataller, M. Braibanti, M. Carpineti, R. Cerbino, F. Croccolo, A. Donev, W. Köhler, J. M. O. de Zárate, and A. Vailati, Eur. Phys. J. E **39**, 119 (2016).
[94] T. R. Kirkpatrick and J. K. Bhattacherjee, Phys. Rev. Fluids **4**, 024306 (2018).
[95] H. S. Samanta, M. L. Mugnai, T. R. Kirkpatrick, and D. Thirumalai, J. Phys. Chem. Lett. **10**, 2788 (2019).
[96] J. M. de Zárate, T. R. Kirkpatrick, and J. V. Sengers, arXiv:1804.06125 (2018).
[97] P. Gaspard and R. Kapral, J. Chem. Phys. **148**, 134104 (2018).
[98] This semianalytical result underestimates by 20% the exact large $\tilde{q}$ behavior, while it reproduces the small $\tilde{q}$ behavior within an error of 2% [13] .